AIAA JOURNAL
Vol. 53, No. 3, March 2015

Accurate Measurement of Nonlinear Liquid Sloshing

Yang Yang,* Zhan-Wei Liu,† and Wen-Xiong Shi*
Beijing Institute of Technology, 100081 Beijing, People's Republic of China
and
Xian-Fu Huang‡
State Key Laboratory of Nonlinear Mechanics, Chinese Academy of Sciences, 100190 Beijing, People's Republic of China

DOI: 10.2514/1.J053676

The accurate measurement of nonlinear liquid sloshing in a liquid-filled spacecraft is of importance for precise flight control. In this paper, a novel noncontact method combining the fringe transmission technique with the liquid-level reflection technique has been developed to accurately evaluate such behavior. To do this, a printed fringe pattern was first placed underneath a transparent test tank with fabricated calibration tails on the wall and, when viewed from above with a high-speed camera, a series of distorted transmission-fringe images with reflected images of the liquid level at different times during the sloshing process were achieved. Combing the quantitative relationship between the shape of the liquid surface and the distortion of the transmission fringes, as well as considering the height curves of the liquid level, the three-dimensional dynamic deformation field could be calculated using multidirectional Newton iterative algorithms. Both the dynamic deformation field of the liquid surface and the residual liquid volume in the tank could be accurately measured at the same time. An experimental verification was carried out, and the results obtained demonstrated the feasibility and reliability of this new method.

Nomenclature

dh	=	height difference
f	=	generic function
H	=	height, mm
h	=	out-of-plane displacement, mm
L	=	length, mm
N	=	node
n	=	refractive index
p	=	height of scattered points
S	=	the in-plane displacement
t	=	time, s
u	=	argument
V	=	volume, ml
x, y, z	=	coordinates
α, β	=	angles
ψ	=	functional

Superscripts

i, j	=	index of coordinates in x and y directions
n	=	number of scattered points

I. Introduction

LIQUID sloshing is of interest in fundamental fluid dynamics and control research, as well as for various practical applications including liquid-filled natural gas carriers, elevated water towers, underground motion when subject to earthquakes, fuel tanks for the automotive industry, and preventing dam breaking [1–8]. This is especially important for the aerospace industry in order to accomplish long and complicated space missions, such as orbit insertion, orbit maintenance, and momentum unload, as modern spacecraft require large amounts of liquid propellant, most of which have high transparency and fluidity. Hence, since the early 1960s, the problem of liquid sloshing dynamics has been of major concern to aerospace engineers studying the influence of liquid propellants sloshing within fuel tanks on the attitude control, performance, and stability of spacecraft [9–15].

The influence of liquid sloshing may hamper critical maneuvers in space, with a series of failures leading to catastrophe, as exemplified by problems that occurred on the ATS-V spacecraft, Intelsat IV series of spacecraft, the NEAR Shoemaker mission, and Gravity Probe B [16]. As the ratio between propellant and dry mass increases, the impact of sloshing also increases. Since the reaction forces and moments caused by fuel sloshing can degrade the pointing accuracy of a control system and impact the stability of the integral structure, it is hence very important to predict its effects.

The challenge of solving such a fascinating problem has attracted the attention of engineers, mathematicians, and scientific researchers over the past few decades. Abramson [3] provided a comprehensive review and discussion of the analytical and experimental studies of liquid sloshing that took place prior to 1966. With the advent of high-speed computers, the numerical approach grew into a new and powerful method to study sloshing. The subsequent maturing of computational techniques, like the finite element method or the boundary element method for the small-scale sloshing and computational fluid dynamics of large-scale sloshing in low gravity, has made contributions toward solving the problem [17–23]. For the experimental study of liquid dynamics and liquid management problems in space, a spacecraft named Sloshsat FLEVO was launched in Geostationary Transfer Orbit as part of the test payload of Ariane 5 Evolution Cryotechnique type A on 12 February 2005. The Sloshsat experiments were designed to give more information on contact line behavior and damping [24,25].

Compared with the theoretical and numerical approach, the experimental investigations have led to novel techniques. The experiments for liquid sloshing usually focus on sloshing wave amplitude, frequency, sloshing force, pressure exerted on the walls, and the effect of sloshing on stability in a container environment. To get this information mentioned above, multiple sensors were developed, such as liquid velocity sensors, accelerometers, and gyroscopes for the Sloshsat FLEVO satellite state measurement [24], wave height sensors made of capacitance probes [26], and pressure transducers or gauges used by Akyildiz and Ünal [27] and Panigrahy et al. [28]. These sensors were deployed on the walls or baffles of tanks for

Received 9 July 2014; revision received 27 August 2014; accepted for publication 28 August 2014; published online 9 January 2015.

*Graduate Student, Department of Mechanics, School of Aerospace Engineering.
†Professor, Department of Mechanics, School of Aerospace Engineering; liuzw@bit.edu.cn (Corresponding Author).
‡Assistant Professor, Institute of Mechanics.

detecting the desired information only at the location of the sensor by using traditional single-point measurement techniques. However, very little information can be obtained about the measurement of the full-field dynamic deformation of a liquid surface for nonlinear liquid sloshing: in particular, in the tanks of space vehicles. As we know, the measurement of the morphology of a free surface can suggest an intuitive understanding in the sloshing phenomenon, in a broader sense, it is also able to provide most of the information such as frequency, vibration modal, amplitude, damper rate, and residual volume in tracing the liquid surface in the tanks. Such specific scientific information has important implications for the study of liquid sloshing dynamics, fluid–structure interactions [29,30], and liquid management problems. Furthermore, it is also significant for the design of tanks, the altitude adjustment of aircraft, and avoiding accidents caused by the liquid sloshing and the stability of liquid-filled spacecraft, as examples.

A great many conventional optical methods for evaluating solid surface topography have failed in this sloshing issue [31,32]. Existing techniques for measuring the three-dimensional (3-D) shape of a deformed liquid surface, like holographic interferometry [33] and holographic shearing interferometry [34], have very high sensitivity and accuracy, but the measurement range is within the sub-millimeter or micrometer scale and is limited by the fringe resolution. On the other hand, the optical path and devices used are complicated. Huang et al. improved the fringe reflection technique by developing monoscopic fringe reflectometry for sensing water wave variations [35]. However, these methods contain some insurmountable limitations, meaning that they are not suitable for measuring specular surfaces with large curvatures. Liu et al. [36] and Shi et al. [37] first proposed the fringe transmission technique (FTT) for measuring liquid surface deformation by analyzing the virtual images of transmission fringes [36,37]; however, this method is generally used for measuring the morphology of deformed liquid surfaces containing at least an undeformed area as the reference, and thus is not suitable for measuring a complete sloshing liquid surface.

A novel method based on the FTT and the liquid-level reflection technique is introduced here for evaluating the dynamic deformation of a liquid surface during nonlinear liquid sloshing. The new measurement method inherits most of the ordinary FTT merits such as a simple setup, high sensitivity, low cost, and full-field and non-contact measurements. The complete relationship between the variation of transmitted light and liquid surface deformation was theoretically and systematically investigated. With this, the new technique, which was verified experimentally, proved to be a feasible method for measuring a sloshing liquid by capturing the transmission fringes and liquid level simultaneously.

II. Measurement Principles of the Three-Dimensional Dynamic Deformation Field of Nonlinear Liquid Sloshing

A. Basic Principles of Fringe Transmission Technique

The FTT for measuring a micro-3-D shape of a deformed liquid surface was first carried out by Liu et al. in 2012 [36]. Figure 1 shows the experimental layout of the method for investigating a deformed liquid surface. The out-of-plane deformation leads to changes of the exit angle of transmitted light from the bottom of the liquid, resulting in a deformation of the virtual image of an object submerged in the liquid. When a periodic fringe is placed in the liquid, the transmitted virtual image will be modulated by the 3-D shape of the liquid, with the transmission-fringe distortion being directly related to the out-of-plane deformation of the liquid surface. As shown in Fig. 1a, for example, point A transfers to point A' when the water surface sinks, whereas the virtual image A' is on the reverse extension line of the refracted ray and on the image plane as observed.

The geometrical relationship between the displacement of a distorted fringe and the height distribution of the liquid surface is presented in Fig. 1b. It is assumed that the deformed curve of the cross section in the liquid surface is simply segmented and approximated into a number of continuous ultrashort polylines at time t, where N_i is the node of the polylines ($i = 1, 2, 3, \ldots$). When the refracted ray of point A is transmitted out of the water surface at the position N_i, Snell's law applies [36,37]:

$$n_w \cdot \sin \beta_i = n_a \cdot \sin \alpha_i \tag{1}$$

where n_w and n_a (usually equal to one) are the refractive indices of water and air; and β_i and α_i are the incidence and emergence angles toward the surface normal, respectively.

The image of point A (prior to deformation) and point A' (transferred from the image of point A) are on the same plane. So, for right triangle A–N_i–A', the geometric relationship is as follows:

$$\begin{cases} H - h(x, y, t) = \frac{S(x,y,t)}{\tan(\alpha_i - \beta_i)} \\ S(x, y, t)|_{x=0} = \beta(x, y, t)|_{x=0} = 0 \end{cases} \tag{2}$$

where H is the initial water depth that can be directly measured; $h(x, y, t)$ is the out-of-plane displacement field of the liquid surface at time t; $S(x, y, t)$ is the in-plane displacement of the virtual image of the underwater fringe at time t, which is the distortion deformation of the transmission-fringe image; and $\angle A$–N_i–$A' = \alpha_i - \beta_i$ (see the cross-section view of the deformed liquid surface curve in Fig. 1b).

In addition, from Fig. 1b, it also can be seen that, in right triangle $N_{i-1} - N_i - P$, the mathematical relations between h and α can be derived using the definition of the integration:

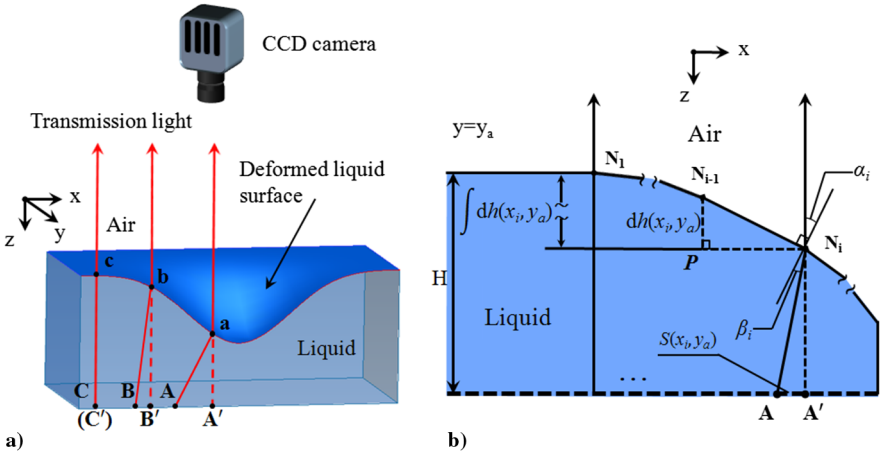

Fig. 1 Representations of a) schematic diagram of the deformed liquid surface; and b) geometrical relationship shown in the cross section. (CCD denotes charge-coupled device.)

$$\begin{cases} h(x,y,t) = \int_0^x \frac{\partial h(x,y,t)}{\partial x}\mathrm{d}x = \int_0^x \tan\alpha \cdot \mathrm{d}x \\ h(x,y,t)|_{x=0} = \left.\frac{\partial h(x,y,t)}{\partial x}\right|_{x=0} = \alpha(x,y,t)|_{x=0} = 0 \end{cases} \tag{3}$$

where in the process of integral computation, y and t are kept constant; x varies; and h and S are functions of x, y, and t.

Combining Eqs. (1) to (3) gives

$$\begin{cases} h(x,y,t) = H - S(x,y,t)\ \Psi\left\{\frac{\partial h(x,y,t)}{\partial x}\right\} \\ \Psi(u) = \frac{\sqrt{n_w^2+(n_w^2-1)\cdot u^2}+u^2}{u\times\{\sqrt{n_w^2+(n_w^2-1)\cdot u^2}-1\}} \\ h(x,y,t)\Big|_{x=0} = \left.\frac{\partial h(x,y,t)}{\partial x}\right|_{x=0} = 0 \end{cases} \tag{4}$$

This is the mathematical basis of the method for measuring liquid surface deformation, which reveals that the 3-D deformation [i.e., $h(x,y,t)$] can be changed into the in-plane displacement measurement of a virtual image of a transmitted fringe, i.e., $S(x,y,t)$ [37].

In the study of Liu et al. [36] and Shi et al. [37], the liquid level of the area away from the tested region does not change during the entire process; this static area of the liquid surface is considered as the reference plane where the initial water depth H can be directly measured. The step height is $h(x,y,t)$, with an initial value of zero in the undeformed liquid plane. The displacement $S(x,y,t)$ for every pixel in the virtual image at time t can be calculated through the distortion of the fringes, and then the height difference between each node $\mathrm{d}h(x,y,t)$ can be calculated point by point using the Newton iteration algorithm along the x direction from the reference plane, which is static. All the profile curves can eventually be obtained to reconstruct the 3-D shape of the water surface at time t using this method.

However, it is more complicated for the case of sloshing within tanks where there is no static reference plane. Additionally, an initial value for an iterative algorithm is needed. Thus, a real full-field dynamic deformation of a liquid surface in nonlinear liquid sloshing cannot be acquired by only using the ordinary FTT. The development of an advanced method for measuring the dynamic deformation of a liquid surface for nonlinear liquid sloshing is imperative.

B. Principle of Three-Dimensional Deformation Measurement Without a Static Reference Plane

The principle of the new method for measuring dynamic deformation of a sloshing liquid surface is to print high-precision orthogonal calibration tails on the wall of a tank along the toroidal and radial directions for recording the dynamic deformation of the liquid level during the sloshing evolution. The curves of the liquid level can then be obtained by interpolation and fitting, and the heights of each curve as initial values can be extracted. Reconstructing the dynamic deformation of a liquid surface by combining the heights of the liquid level and the iterative algorithm based on the relationship between the variation of the fringes and liquid surface deformation has been cited from literature [37].

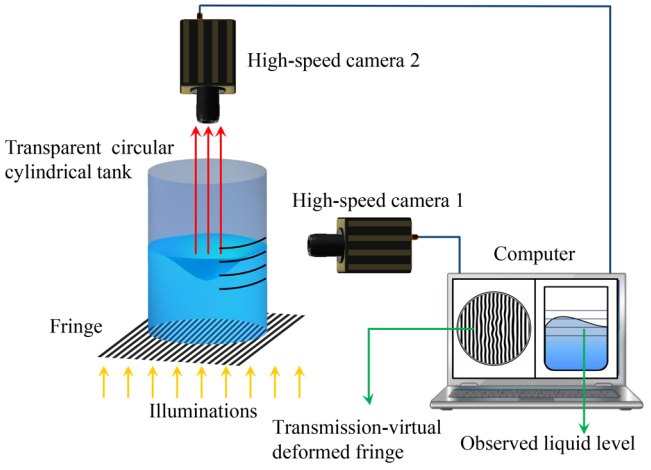

Fig. 2 Layout of measuring the deformation of a sloshing liquid surface without a static reference plane.

As an example, the liquid motion in an upright transparent circular cylindrical tank was used to demonstrate the principle and layout for measuring the deformation of a sloshing liquid surface without a static reference plane, as shown in Fig. 2. Besides the periodic fringe placed under the tank, high-precision orthogonal calibration tails could printed, drawn, or pasted on the wall along the toroidal and radial directions as a scale for height and position coordinates. For performing the iterative algorithm, the observed toroidal calibration tails must be orthorhombic with the principal direction of the fringe. As presented in Fig. 2, high-speed camera 1 is set up horizontally for recording the height of the contact line between the free surface and the vertical wall; and high-speed camera 2 is set up vertically, making the target surface of the camera parallel with the fringe pattern for recording the distortion of the transmission fringes. Images of the height of the contact line and distortions of the transmission fringes are hence captured by two high-speed cameras simultaneously and continuously during sloshing. The images are then recorded for computation and analysis. It should be noted that, before the sloshing, a transmission-fringe pattern should be acquired as a carrier fringe pattern at the time the liquid surface is flat. Displacement calculated from the transmission-fringe patterns subtracts the displacement of the carrier fringe pattern to obtain a distortion displacement field at each time, i.e., to obtain displacements $S(x,y,t)$ of each point on the transmission fringe. As stated previously, when sloshing occurs in a tank, the liquid-level height is not fixed and the initial value at the tank edge is not zero, so the height of the contact line between free surface and the vertical wall needs to be calibrated and acquired at each point at each time. In this paper, the height of some scattered points selected from the contact lines are calibrated as $p_1, p_2, p_3, \ldots, p_n$ by the calibration tails with an interpolation algorithm. In this way, the height of each pixel $H(x,y,t)$ at the contact lines as initial values for iterative algorithm will be obtained. Combining Eq. (4) gives

$$\begin{cases} h(x,y,t) = H(x,y,t) - S(x,y,t)\ \Psi\left\{\frac{\partial h(x,y,t)}{\partial x}\right\} \\ \Psi(u) = \frac{\sqrt{n^2+(n^2-1)\cdot u^2}+u^2}{u\times\{\sqrt{n^2+(n^2-1)\cdot u^2}-1\}} \\ H(x,y,t) = f(p_1, p_2, p_3, \ldots, p_n) \end{cases} \tag{5}$$

where $n = n_l/n_g$; n_1 is the refractive index of the liquid in the tank; n_g is the refractive index of the ambient gas; and

$$h(x,y,t)|_{x=t=0} = \left.\frac{\partial h(x,y,t)}{\partial x}\right|_{x=t=0} \neq 0$$

is the sloshing condition. Putting the height of one point on the contact line $H(x,y,t)$ and the displacement $S(x,y,t)$ of this corresponding point for the transmission fringe in the principal direction into Eq. (5), the height difference of the next point $\mathrm{d}h(x,y,t)$ can be obtained and put into the calculation of the third point. An iterative algorithm is performed along the x direction to obtain the height difference between the deformed liquid level and the initial liquid surface of this cross section in the z direction. According to this method, all of the out-of-plane deformed displacements of different points along the y direction can be obtained, eventually reconstructing the liquid surface morphology over time.

To save experimental costs and improve efficiency, the measurement principle and system have been further improved by using only a single high-speed camera for data acquisition. On the basis of the required initial data, the displacement of transmission fringes, and the liquid level of a free surface, a flat mirror at a certain angle was used for changing the vertical direction of the images of the wall into the horizontal direction. With this monoscopic method, information in different dimensions could be captured in one dimension simultaneously.

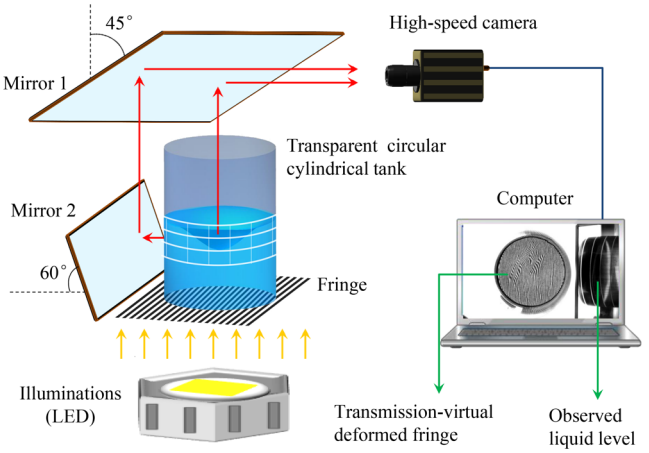

Fig. 3 Schematic of the improved experimental setup for a monoscopic method.

Figure 3 illustrates the improved experimental setup for a monoscopic method. Mirror 1 is placed at an angle of 45 deg, with the vertical direction above the transparent circular cylindrical tank. A single high-speed camera is mounted horizontally toward mirror 1. A rectangular mirror (mirror 2) is placed beside the tank at an angle about 50 to 60 deg in the horizontal direction, which is used to reflect the image of at least half a wall of the tank. It should be noted that the lower edge of mirror 2 needs to be strictly vertical with the principal direction of the fringe pattern. By adjusting the angle of these two mirrors, the image of the distorted transmission fringes and liquid level of the free surface will be reflected in the horizontal direction and captured by the single high-speed camera simultaneously; these images will be displayed in the same field of view.

Since this improved method has been adopted, the approach has been found to be more suitable for detecting the dynamic deformation of a continuous surface for nonlinear liquid sloshing, which has no static reference plane during its shape variation. Furthermore, this developed method is outstanding not only for its cost reduction (easily obtaining all of the required information that, in different dimensions, can only be collected by a single high-speed camera) but also provides a powerful approach to avoid synchronization issues for two high-speed cameras as well as reducing systematic errors. For future work, if needed, multiple sets of flat mirrors or a horn-shaped mirror could be used around the tank for capturing more images of the liquid level to acquire a rich set of initial values of an iterative algorithm, to improve the accuracy.

III. Validation Test

A. Experimental Setup and Procedure

A validation test was performed in a transparent circular cylindrical tank in normal gravity and air conditions, as illustrated in Fig. 3. The open tank was made of glass and had an inner diameter of 71 mm. Red wine of 12% alcohol content was used to imitate transparent propellant (for instance, hydrazine, kerosene, and furfuryl alcohol) as its properties, such as transparency, viscosity, surface tension, etc., are similar, and it has the advantage of enhancing the contrast, hence being more suitable than water. The height of the static liquid surface before sloshing was 25.23 mm. The refractive index of the liquid n_1 was 1.340, and the refractive index of the glass used for the tank was $\sqrt{2}$, which was ignored in subsequent calculations because the glass was very thin. The periodic fringe pattern used in the experiment had a frequency of 0.66 lines/mm. High-precision orthogonal calibration tails printed on the wall along the toroidal and radial directions as the scale of height and position coordinates were used for obtaining the height of the liquid level at each point by physical or digital interpolation, with spacing of 10 and 1 mm, respectively.

A high-speed camera (Photron FastCam SA1.1), with a Nikon AF-Nikkor 50 mm 1 : 1.4D lens, was used for the image acquisition. The camera speed was set to 1000 frames per second at its full resolution of 1024×1024 pixels. To remove the specular reflection at the interface, polarizers were placed in front of the lens. If the deformation of the surface was too large, a double-telecentric lens (Schneider Kreuznach Xenoplan 1 : 5 0.13/11) could also be used to avoid severe defocus phenomenon.

As the exposure time of the camera was very short, an even, efficient, and high level of illumination would be required such that it should be in pure dc operation to eliminate strobing. In this investigation, a 150 W dc light-emitting diode (LED) illuminator was mounted vertically underneath the periodic fringe pattern, making the high-speed acquisition clearer.

The procedure designed for the experiment was as follows:

1) The experimental system (transparent circular cylindrical tank, light illuminators, high-speed camera, lens, mirrors 1 and 2, and other optical instruments) was established according to the experimental layout in Fig. 3.

2) A physical periodic fringe was placed under the transparent circular cylindrical tank partly filled with liquid, with its size and frequency preset as required.

3) The angles of mirrors 1 and 2, the position of the camera, the focal length, the aperture size, and other parameters of the lens were all adjusted to ensure the observed frames were clear and displayed in a same field of view.

4) An original transmitted fringe image was captured when the liquid surface was flat, as a reference for subsequent calculations and elimination of environmental factors on the final results.

5) Blowing abruptly through a straw into the tank generated liquid sloshing. It should be noted that deformation and relative position deviation between the fringe, calibration tails, and camera were forbidden in the sloshing process.

6) A series of distorted transmitted fringe images and liquid-level images were recorded during the sloshing evolution for computation.

B. Measurement Results and Discussion

Figure 4 shows an instantaneous image of a distorted transmission-fringe pattern and liquid-level information. A magnified view of the observed liquid level is demonstrated in Fig. 4c. The line connecting the numbers is the contact line between the free surface and the wall of the tank in Fig. 4c. The heights of the scattered points selected from the contact lines are $p_1, p_2, p_3, \ldots, p_n$, and they were calibrated by the calibration tails with an interpolation method. There have been various interpolation methods used to implement into the calibration. In this paper, image-processing software was used to obtain the coordinates of all the scattered points as well as the separation distance between each adjacent toroidal calibration tail. Since the real spacing of the calibration tails was known, the real height of each scattered point on the contact line can be calculated via the corresponding conversion. Then, the height of all the continuous pixels $H(x, y, t)$ for the contact line could be obtained by one-dimensional interpolation (the cubic spline interpolation was used in this study) operated upon the scattered points. Profiles of the observed liquid level at different moments are plotted in Fig. 5. A wetting phenomena occurred in the liquid–solid contact during the test; when reading a depth scale on the side of a tank filled with liquid, the fluid meniscus must be taken into account in order to obtain an accurate measurement [38]. Hence, in the process of calibration, the difference in heights between the contact line and the free surface should be considered carefully due to the surface tension (approximately 1 mm in this study).

Another part of the experimental data needed is the displacement of the transmission fringe. Images of the distorted transmission fringes at different times are presented in Fig. 6. Preprocessing of the fringe patterns such as image smoothing, denoising, and contrast enhancement will facilitate the subsequent processing. Image space transformation was also performed to establish a global context structure for the images. The centerline of the fringes can then be exacted by Moiré analysis software [39]. Besides, a transmission-fringe pattern should be acquired as a carrier fringe pattern when the liquid surface is flat. After the ordering and interpolating of the

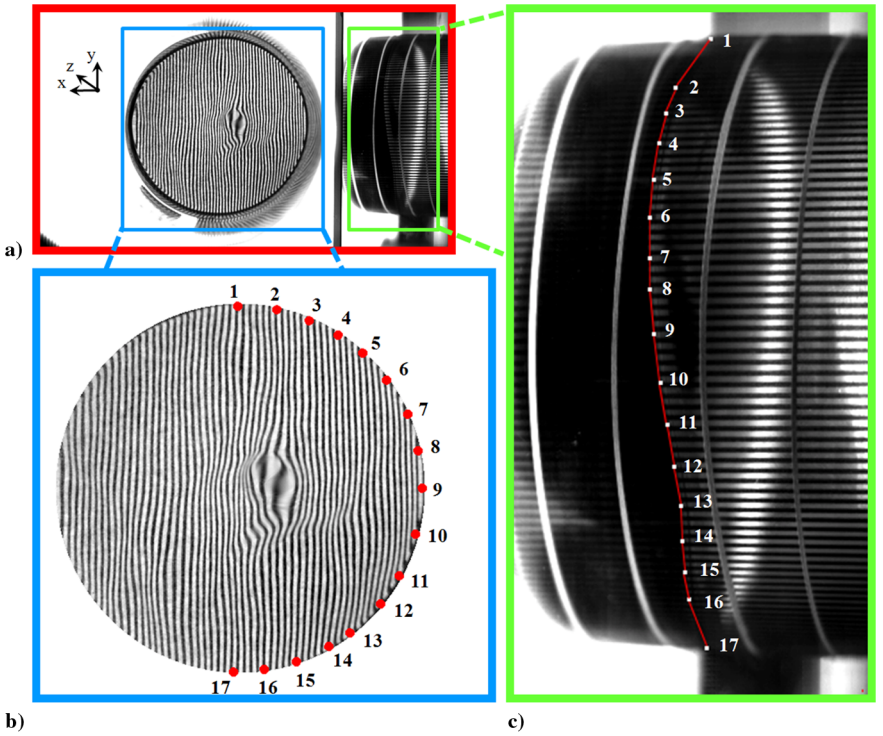

Fig. 4 Representations of a) instantaneous image captured by a high-speed camera, b) distorted transmission-fringe pattern, and c) the observed liquid level.

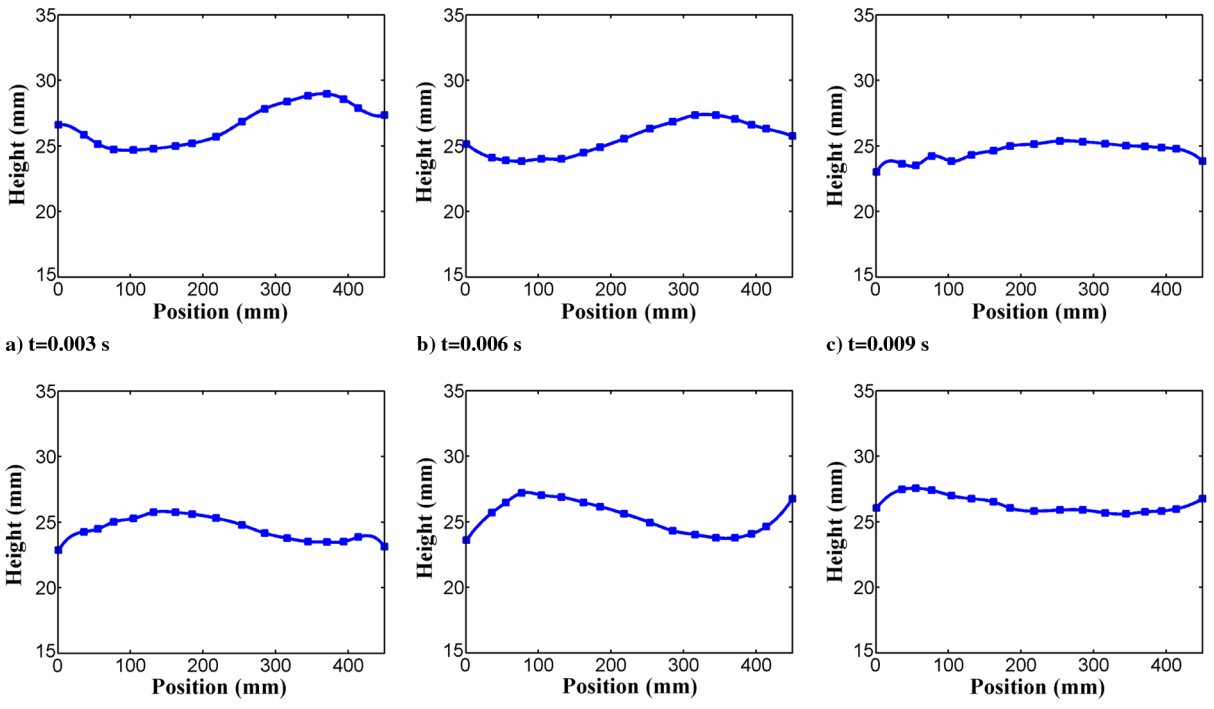

Fig. 5 Profiles of the observed liquid level at different times.

thinned fringe patterns, calculating the full-field displacement of the deformed transmission-virtual fringes and subtracting the virtual displacement from the carrier fringes, full-field displacement of the deformed transmission fringe can be achieved. The displacement distribution image is shown in Fig. 7.

Put the height $H(x, y, t)$ of one point on the contact line and the displacement $S(x, y, t)$ of the corresponding point for the transmission fringe in the principal direction, which were calculated as shown previously, into Eq. (5). The height difference $\mathrm{d}h(x, y, t)$ of the next point can then be obtained and put into the calculation of the third point. Here, the Newton iteration was used pixel by pixel to work out the displacement of the deformed liquid in the z direction and, eventually, reconstruct the liquid surface morphology at different times. After frame-by-frame reconstruction, the dynamic scene of the liquid sloshing can be digitalized. Here, six frames of the typical 3-D shape results from 0.003 to 0.018 s with an interval of 0.003 s are shown in Fig. 8, from which the evolution of nonlinear liquid sloshing is demonstrated. Figure 9 shows profiles of the free

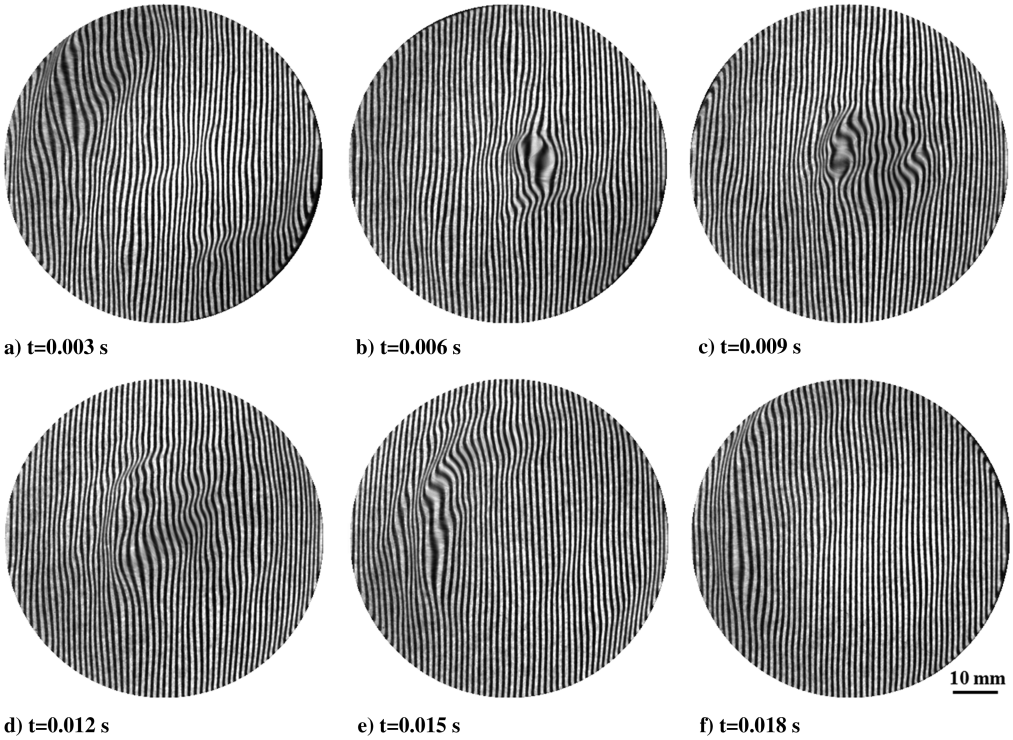

a) t=0.003 s b) t=0.006 s c) t=0.009 s

d) t=0.012 s e) t=0.015 s f) t=0.018 s

Fig. 6 Images of the distorted transmission fringe at different times.

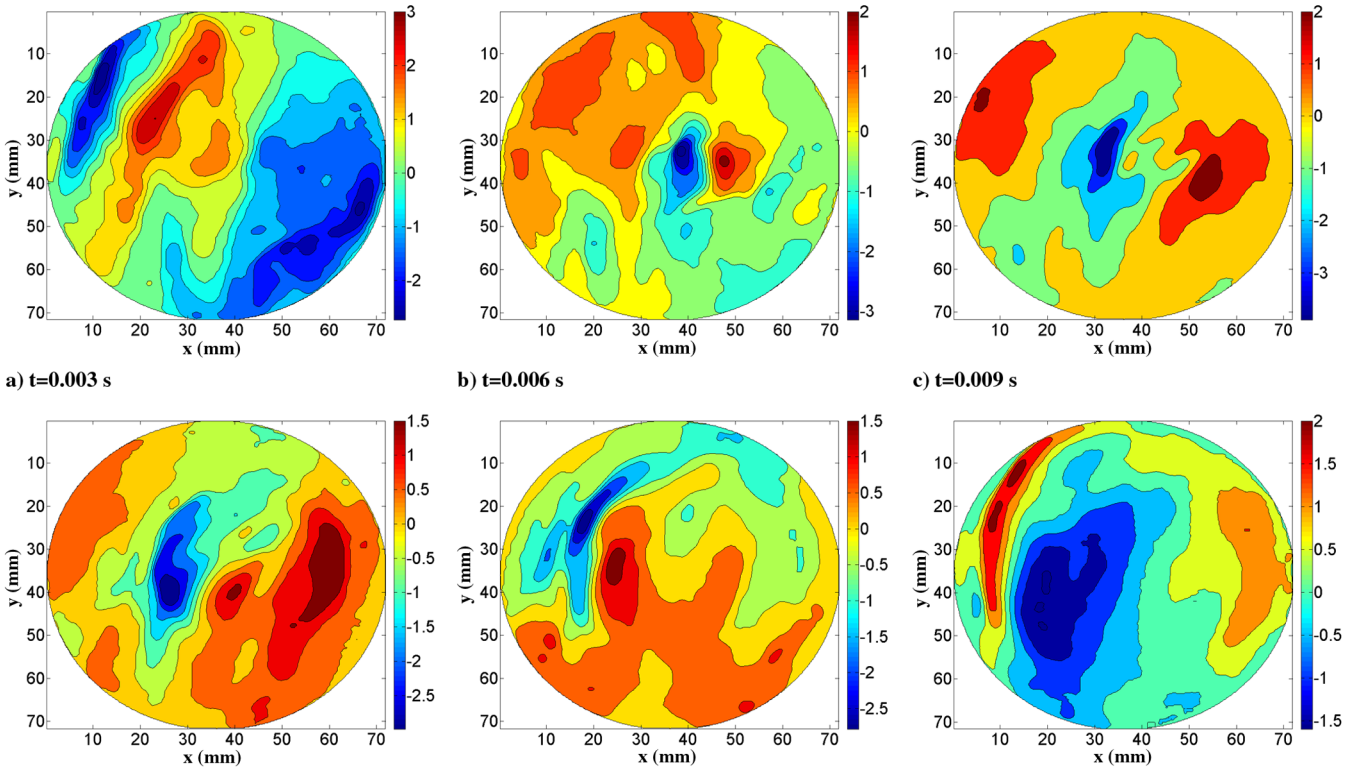

a) t=0.003 s b) t=0.006 s c) t=0.009 s

d) t=0.012 s e) t=0.015 s f) t=0.018 s

Fig. 7 Displacement distribution images at different times.

surface measured for the dynamic liquid wave along the *y* direction. The measurement results indicated that the largest amplitude of the sloshing liquid was approximately 18.7% of the radius of the liquid-filled tank. As displayed in Figs. 8a, 8b, and 8c, when blowing into the tank, the liquid surface sinks at the beginning and then surges and rises with some ripples occurring around the peak. After some up and down motions, the waves quickly die out and the liquid surface subsides gradually, as shown in Figs. 8d through 8f. Combining Figs. 8 and 9, there is no flat area on the surface that can be observed during the whole sloshing process. Besides, the amplitude and vibration modes, and so on, will be obtained by the morphology of the liquid surface measured beforehand. Cited from the literature

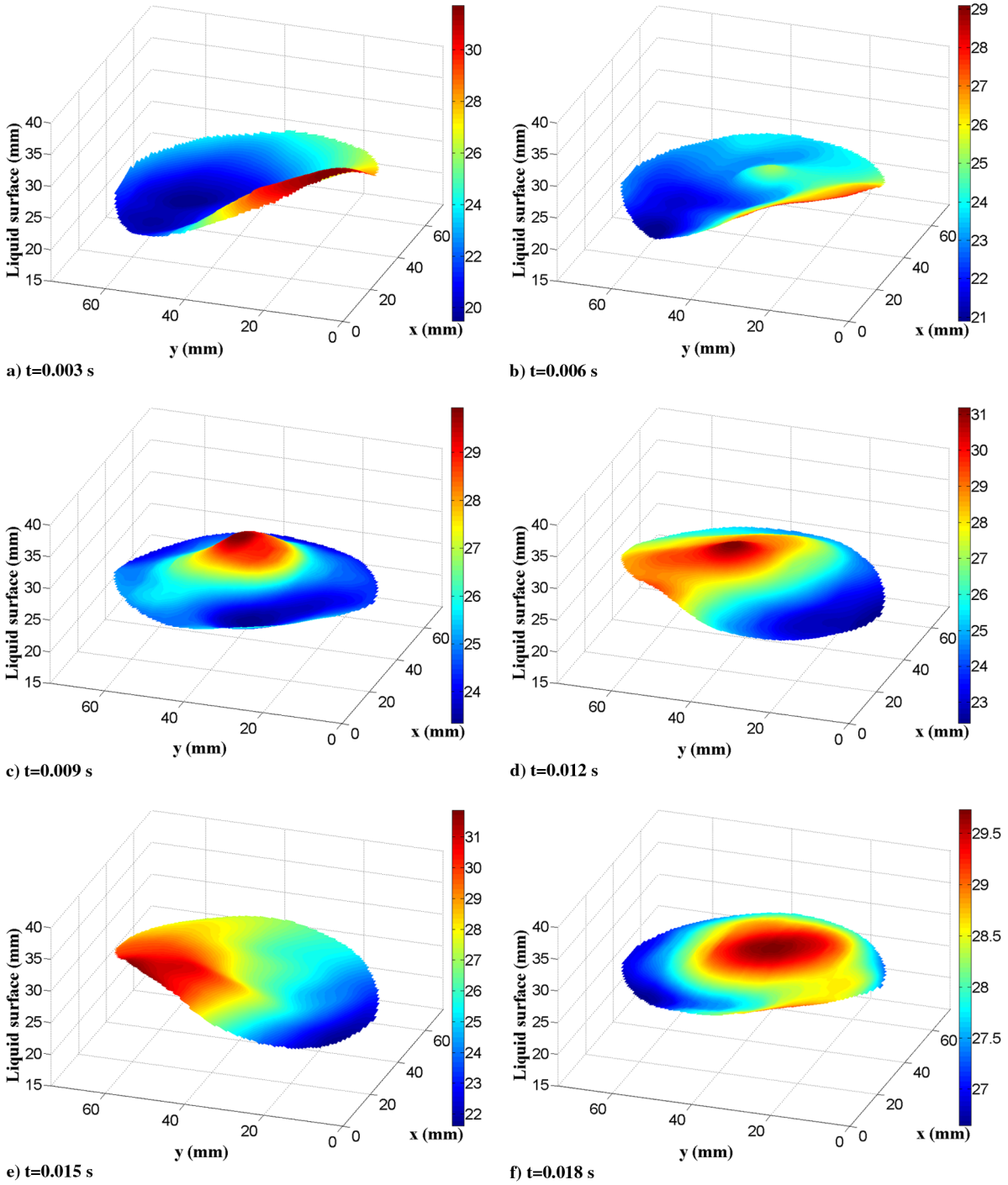

Fig. 8 Evolution of a liquid surface in nonlinear liquid sloshing measured at different times.

[40], the sensitivity of the fringe center method is 10% of the fringe spacing. In this experiment, by Eq. (5), the sensitivity of measuring the liquid surface height is better than 4.0 μm under the condition of a fringe frequency of 0.66 lines/mm with a calculation step of 0.167 mm and a static liquid depth of 25.23 mm. A liquid can be idealized as incompressible; thus, the volume of liquid in the tank can be estimated as a constant during sloshing. Hence, such a process was demonstrated to verify the validity of the method as follows. The real volume of liquid in the tank is 99.89 ml, and the volume V at different times during sloshing can be calculated through the height of each point on the free surface, which is given in Eq. (6):

$$V = \sum_{i=1}^{m} \sum_{j=1}^{n} L_i \times L_j \times h_{ij} \tag{6}$$

The surface is divided into numerous microregions (m rows and n columns), where L_i refers to the length of the ith row and L_j refers to the length of the jth column, and they are related to the computing precision (where $L_i = L_j = L$ is the step length that influences the accuracy of the calculation). The area of the ith row and jth column of the small region is $L_i \times L_j$, and the distance between the liquid surface and the bottom is h_{ij} [herein, $h_{ij} = h(x, y, t)$].

Table 1 lists the calculated volume of liquid and the error and relative error at different times. These errors may mainly be caused by a number of factors, such as the actual difference in height between the concave and convex surface being less than 1 mm of the liquid-level measurement; the cylindrical bottom of the tank not being perfectly round but being treated as a perfect circle in postprocessing; the accumulation of calculation errors and lens distortion; and so on. However, the average relative error is only 4.0%, indicating that the developed method is feasible and reliable.

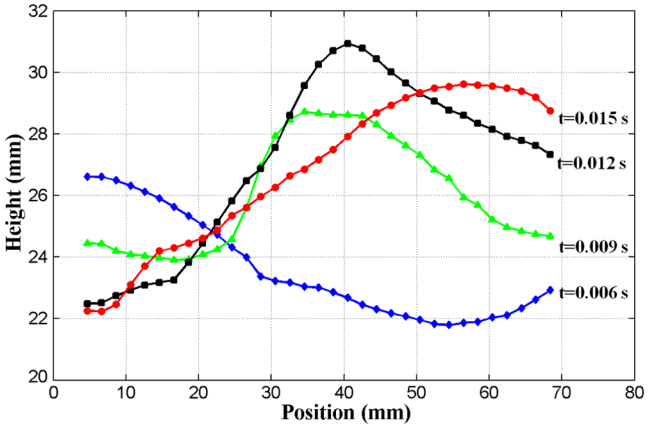

Fig. 9 Profiles of a free surface measurement for a dynamic liquid wave along the *y* direction.

IV. Conclusions

A real-time and noncontact method has been proposed for measuring the full-field 3-D dynamic deformation of a liquid surface in nonlinear sloshing. The new method, combining the fringe transmission technique with the liquid-level reflection technique, has solved the problem of measuring the real-time deformation measurement for a sloshing liquid surface that has no static reference plane. In this paper, the basic principle has been thoroughly explored and the theoretical equation for the 3-D liquid surface morphology measurement was derived mathematically. A special fringe pattern was placed underneath the transparent tank, fabricated calibration tails were placed on the wall of the tank, and a single high-speed camera was mounted above the tank to capture a series of distorted transmission-fringe images and reflected images of a liquid level at different times during sloshing evolution. The quantitative relationship between the shape of the liquid surface and the distortion of transmission fringes was applied to obtain the relative deformation of the liquid surface at different times and extract the fitted height curves of the liquid level at different times on the contact lines as the initial values; the full-field dynamic deformation of a liquid surface can be calculated using the Newton iteration algorithm. The method can accurately measure the dynamic deformation of a liquid surface for nonlinear liquid sloshing, and it is able to achieve the accurate measurement of residual liquid volume in the tank. Furthermore, it has the potential for investigating the vibration mode and frequency. Exploratory experiments have been conducted for the dynamic deformation of a liquid surface caused by propellant sloshing in the tank of a spacecraft in normal gravity, which have successfully demonstrated the feasibility and reliability of this method. Since the whole measuring system requires only one high-speed camera while collecting deformation information about the transmission surface and lateral liquid level, the whole system has the characteristics of a compact structure with low cost. Meanwhile, the developed method is outstanding for its ease of operation and minimal effect on the measured object, as well as high sensitivity. It provides a new approach for relevant researchers in the area of dynamic characteristics of liquid sloshing in the tank of space vehicles in the future.

Table 1 Calculated volume of liquid and its error and relative error at different times

	Volume, ml	Error, ml	Relative error, %
$V_{t=0.003\ s}$	97.86	2.14	2.0
$V_{t=0.006\ s}$	97.76	2.24	2.1
$V_{t=0.009\ s}$	102.70	2.70	2.8
$V_{t=0.012\ s}$	106.70	6.70	6.8
$V_{t=0.015\ s}$	104.53	4.53	4.6
$V_{t=0.018\ s}$	94.27	5.73	5.6

Acknowledgments

The authors are grateful to the financial support from the National Natural Science Foundation of China (nos. 91216301, 11232008, 11072033, and 11372037), the Program for New Century Excellent Talents in University (NCET-12-0036), and the Natural Science Foundation of Beijing (grant no. 3122027).

References

[1] Ibrahim, R. A., Ikeda, T., and Pilipchuk, V. N., "Recent Advances in Liquid Sloshing Dynamics," *Applied Mechanics Reviews*, Vol. 54, No. 2, 2001, pp. 133–199. doi:10.1115/1.3097293

[2] Rumold, W., "Modeling and Simulation of Vehicles Carrying Liquid Cargo," *Multibody System Dynamics*, Vol. 5, No. 4, 2001, pp. 351–374. doi:10.1023/A:1011425305261

[3] Abramson, H. N. (ed.), "The Dynamic Behavior of Liquids in Moving Containers," NASA SP-106, 1966.

[4] Dodge, F. T., *The New 'Dynamic Behavior of Liquids in Moving Containers'*, Southwest Research Inst., San Antonio, TX, 2000, pp. 111–116.

[5] Abramson, H. N., "Dynamics of Contained Liquids: A Personal Odyssey," *Applied Mechanics Reviews*, Vol. 56, No. 1, 2003, pp. R1–R7. doi:10.1115/1.1511517

[6] Ibrahim, R. A., "Liquid Sloshing Dynamics," *Theory and Applications*, Cambridge Univ. Press, New York, 2005, pp. 497–682.

[7] Bauer, H. F., "Theory of Liquid Sloshing in Compartmented Cylindrical Tanks Due to Bending Excitation," *AIAA Journal*, Vol. 1, No. 7, 1963, pp. 1590–1596. doi:10.2514/3.1862

[8] Farhat, C., Chiu, E. K. Y., Amsallem, D., Schotté, J. S., and Ohayon, R., "Modeling of Fuel Sloshing and its Physical Effects on Flutter," *AIAA Journal*, Vol. 51, No. 9, 2013, pp. 2252–2265. doi:10.2514/1.J052299

[9] Morgenstern, W. M., et al., "Solar Dynamics Observatory Guidance, Navigation, and Control System Overview," *AIAA Guidance, Navigation, and Control Conference*, AIAA Paper 2011-6726, 2011, pp. 8–11.

[10] Baeten, A., and Juettner, C., "Orbit Insertion Dynamics of a Picosatellite with Respect to Coupled Solid-Liquid Dynamics," AIAA Paper 2011-0391, 2011.

[11] Silvernail, N. L., Sances, D. J., and Gangadharan, S., "Modeling of Fuel Slosh in a Spin Stabilized Spacecraft with On-Axis Propellant Tanks Implemented with Diaphragms," *AIAA Modeling and Simulation Technologies Conference*, AIAA Paper 2009-6040, 2009.

[12] Veldman, A. E. P., Gerrits, J., Luppes, R., Helder, J. A., and Vreeburg, J. P. B., "The Numerical Simulation of Liquid Sloshing on Board Spacecraft," *Journal of Computational Physics*, Vol. 224, No. 1, 2007, pp. 82–99. doi:10.1016/j.jcp.2006.12.020

[13] Peterson, L. D., Crawley, E. F., and Hansman, R. J., "Nonlinear Fluid Slosh Coupled to the Dynamics of a Spacecraft," *AIAA Journal*, Vol. 27, No. 9, 1989, pp. 1230–1240. doi:10.2514/3.10250

[14] Henderson, D. M., and Miles, J. W., "Surface-Wave Damping in a Circular Cylinder with a Fixed Contact Line," *Journal of Fluid Mechanics*, Vol. 275, Sept. 1994, pp. 285–299. doi:10.1017/S0022112094002363

[15] Yue, B. Z., "Study on the Chaotic Dynamics in Attitude Maneuver of Liquid-Filled Flexible Spacecraft," *AIAA Journal*, Vol. 49, No. 10, 2011, pp. 2090–2099. doi:10.2514/1.J050144

[16] Vreeburg, J. P., "Spacecraft Maneuvers and Slosh Control," *IEEE Control Systems*, Vol. 25, No. 3, 2005, pp. 12–16. doi:10.1109/MCS.2005.1432593

[17] Rebouillat, S., and Liksonov, D., "Fluid–Structure Interaction in Partially Filled Liquid Containers: A Comparative Review of Numerical Approaches," *Computers and Fluids*, Vol. 39, No. 5, 2010, pp. 739–746. doi:10.1016/j.compfluid.2009.12.010

[18] Celebi, M. S., and Akyildiz, H., "Nonlinear Modeling of Liquid Sloshing in a Moving Rectangular Tank," *Ocean Engineering*, Vol. 29, No. 12, 2002, pp. 1527–1553. doi:10.1016/S0029-8018(01)00085-3

[19] Liu, D., and Lin, P., "A Numerical Study of Three-Dimensional Liquid Sloshing in Tanks," *Journal of Computational Physics*, Vol. 227, No. 8, 2008, pp. 3921–3939. doi:10.1016/j.jcp.2007.12.006

[20] Gómez-Goñi, J., Garrido-Mendoza, C. A., Cercós, J. L., and González, L., "Two Phase Analysis of Sloshing in a Rectangular Container with Volume of Fluid (VOF) Methods," *Ocean Engineering*, Vol. 73, Nov. 2013, pp. 208–212. doi:10.1016/j.oceaneng.2013.07.005

[21] Wei, W., Junfeng, L., and Tianshu, W., "Modal Analysis of Liquid Sloshing with Different Contact Line Boundary Conditions Using FEM," *Journal of Sound and Vibration*, Vol. 317, No. 3, 2008, pp. 739–759. doi:10.1016/j.jsv.2008.03.070

[22] Pal, N. C., Bhattacharyya, S. K., and Sinha, P. K., "Non-Linear Coupled Slosh Dynamics of Liquid-Filled Laminated Composite Containers: A Two Dimensional Finite Element Approach," *Journal of Sound and Vibration*, Vol. 261, No. 4, 2003, pp. 729–749. doi:10.1016/S0022-460X(02)01011-8

[23] Rebouillat, S., and Liksonov, D., "Fluid–Structure Interaction in Partially Filled Liquid Containers: A Comparative Review of Numerical Approaches," *Computers and Fluids*, Vol. 39, No. 5, 2010, pp. 739–746. doi:10.1016/j.compfluid.2009.12.010

[24] Prins, J. J. M., "SLOSHSAT FLEVO Facility for Liquid Experimentation and Verification in Orbit Description of the Mini Satellite," National Aerospace Laboratory NLR Techical Publ. 2000-630, Amsterdam, 2000.

[25] Vreeburg, J. P. B., "Measured States of Sloshsat FLEVO," *Proceedings of the 56th International Astronautical Congress* [CD-ROM], Paper 05-C1.2.09, Fukuoka, 2005.

[26] Pal, N. C., Bhattacharyya, S. K., and Sinha, P. K., "Experimental Investigation of Slosh Dynamics of Liquid-Filled Containers," *Experimental Mechanics*, Vol. 41, No. 1, 2001, pp. 63–69. doi:10.1007/BF02323106

[27] Akyildiz, H., and Ünal, E., "Experimental Investigation of Pressure Distribution on a Rectangular Tank Due to the Liquid Sloshing," *Ocean Engineering*, Vol. 32, No. 11, 2005, pp. 1503–1516. doi:10.1016/j.oceaneng.2004.11.006

[28] Panigrahy, P. K., Saha, U. K., and Maity, D., "Experimental Studies on Sloshing Behavior Due to Horizontal Movement of Liquids in Baffled Tanks," *Ocean Engineering*, Vol. 36, No. 3, 2009, pp. 213–222. doi:10.1016/j.oceaneng.2008.11.002

[29] Morand, H. J. P., and Ohayon, R., *Fluid Structure Interaction*, Wiley, Hoboken, NJ, 1995, Chaps. 3, 6, 9.

[30] Andrianarison, O., and Ohayon, R., "Compressibility and Gravity Effects in Internal Fluid–Structure Vibrations: Basic Equations and Appropriate Variational Formulations," *Computer Methods in Applied Mechanics and Engineering*, Vol. 195, No. 17, 2006, pp. 1958–1972. doi:10.1016/j.cma.2004.12.032

[31] Li, C. W., Liu, Z. W., Xie, H. M., and Wu, D., "Novel 3-D SEM Moiré Method for Micro Height Measurement," *Optics Express*, Vol. 21, No. 13, 2013, pp. 15,734–15,746. doi:10.1364/OE.21.015734

[32] Dong, X., Zhang, C., Feng, X., and Hwang, K. C., "Full-Field Measurement of Topography and Curvature by Coherent Gradient Sensing Method at High Temperature," *Experimental Mechanics*, Vol. 53, No. 6, 2013, pp. 959–963. doi:10.1007/s11340-013-9713-x

[33] Hinsch, K. D., "Holographic Interferometry of Surface Deformations of Transparent Fluids," *Applied Optics*, Vol. 17, No. 19, 1978, pp. 3101–3107. doi:10.1364/AO.17.003101

[34] Matsuda, K., Watanabe, S., and Eiju, T., "Real-Time Measurement of Large Liquid Surface Deformation Using a Holographic Shearing Interferometer," *Applied Optics*, Vol. 24, No. 24, 1985, pp. 4443–4447. doi:10.1364/AO.24.004443

[35] Huang, L., Ng, C. S., and Asundi, A. K., "Dynamic Three-Dimensional Sensing for Specular Surface with Monoscopic Fringe Reflectometry," *Optics Express*, Vol. 19, No. 13, 2011, pp. 12,809–12,814. doi:10.1364/OE.19.012809

[36] Liu, Z. W., Huang, X. F., and Xie, H. M., "A Novel Orthogonal Transmission-Virtual Grating Method and Its Applications in Measuring Micro 3-D Shape of Deformed Liquid Surface," *Optics and Lasers in Engineering*, Vol. 51, No. 2, 2013, pp. 167–171. doi:10.1016/j.optlaseng.2012.08.009

[37] Shi, W. X., Huang, X. F., and Liu, Z. W., "Transmission-Lattice Based Geometric Phase Analysis for Evaluating the Dynamic Deformation of a Liquid Surface," *Optics Express*, Vol. 22, No. 9, 2014, pp. 10,559–10,569. doi:10.1364/OE.22.010559

[38] Hu, D. L., and Bush, J. W., "Meniscus-Climbing Insects," *Nature*, Vol. 437, No. 7059, 2005, pp. 733–736. doi:10.1038/nature03995

[39] Wang, Z. Y., "Development and Application of Computer-Aided Fringe Analysis," Ph.D. Dissertation, Mechanical Engineering Dept., Maryland Univ., College Park, MD, 2003.

[40] Dai, F. L., and Wang, Z. Y., "Automatic Fringe Patterns Analysis Using Digital Processing Techniques: I, Fringe Center Method," *Acta Photonica Sinica*, Vol. 28, No. 8, Aug. 1999, pp. 700–706 (in Chinese).

R. Ohayon
Associate Editor